Title: Hydroxyapatite-based cements induce different apatite formation in radicular dentin.

Authors: Manuel Toledano-Osorio[a], Fátima S. Aguilera[a], Raquel Osorio[a*], Esther Muñoz-Soto[a], Mayra C. Pérez-Álvarez[b], Modesto T. López-López[c], Christopher D. Lynch[d], Manuel Toledano[a]

Institution: [a]University of Granada, Faculty of Dentistry, Dental Materials Section.

Colegio Máximo de Cartuja s/n

18071 – Granada - Spain.

[b]University of La Havana, Biomaterials Department.

San Lázaro y L. Municipio Plaza de la Revolución

La Havana- Cuba.

[c]University of Granada, Faculty of Science, Applied Physics Department.

Av. Fuente Nueva s/ n 18071 Granada - Spain.

[d]University Dental School & Hospital/ University College Cork, Wilton, Cork – Ireland

*Corresponding author: Prof. Raquel Osorio

University of Granada, Faculty of Dentistry

Dental Materials Section

Colegio Máximo de Cartuja s/n

18071 – Granada - Spain.

Tel.: +34-958243789

Fax: +34-958240809

Email: rosorio@ugr.es

Acknowledgements

This work was supported by the Ministry of Economy and Competitiveness (MINECO) and European Regional Development Fund (FEDER) Project MAT2017-85999-P. The authors thank the technical support of Álvaro Carrasco-Carmona for manuscript edition.

Declaration of interest: None.

Abstract

Objectives. To investigate crystallinity and ultrastructure of the formed hydroxyapatite at radicular cervical and apical dentin after being treated with three different canal sealers.

Methods. Cervical and apical root dentin surfaces were treated with two experimental hydroxyapatite-based sealers, containing sodium hydroxide (calcypatite) or zinc oxide (oxipatite) and an epoxy resin-based canal sealer (AH Plus); gutta-percha without sealer was included as control. Dentin surfaces were studied by X-ray diffraction and transmission electron microscopy through selected area diffraction and bright-field imaging after 24 h and 12 m of storage.

Results. Root cervical dentin treated with calcypatite and oxipatite produced poor crystallinity of new minerals, wide amorphous phase and non-stoichiometry. Reflections at the 002 plane and the corresponding diffraction rings attained lower values in the Scherrer equation and the Scherrer-Wilson equation in samples treated with both HAp-based sealers than in specimens without sealer or with AH Plus. At root cervical dentin treated with calcypatite, shorter and wider crystallite size formations and lower crystals grain size were found, if compared to those encountered at oxipatite treated dentin. Oxipatite attained improved crystallographic atomic order and less structural variation in both distances and angles. Apical dentin treated with oxipatite attained preferred grain orientation with polycrystalline lattices.

Significance. The immature crystallites formed in dentin treated with calcypatite and oxipatite will account for high hydroxyapatite solubility and remineralizing activity. New polycrystalline formations encountered in apical dentin treated with oxipatite may also produce high mechanical performance.

Hydroxyapatite-based cements induce different apatite formation in radicular dentin

Keywords: Crystallinity; dentin; microscopy; remineralization; TEM; XRD.

1. Introduction

Fractures are frequently encountered in teeth that have been endodontically treated and restored [1]. The susceptibility of the root to fracture is increased after the endodontic treatment [1]. The availability of canal sealers able to strengthen the radicular dentin is a requirement for the current root canal therapy. Proposed materials range from the use of glass-ionomers [2], Portland-based Mineral Trioxide Aggregate cements (MTA) [3], or root canal sealers based on epoxy resins such as AH-Plus [4], but most of them have shown different clinical shortcomings [5]. Calcium hydroxide powder in association with hydroxyapatite (HAp), have been proposed for repair and regeneration of hard tissues [6]. Nevertheless, HAp possesses low mechanical strength and fracture toughness, which is an obstacle for its application in load-bearing structures [6], as root dentin [7]. Zn-substituted HAp has been shown to possess improved mechanical performance and enhanced bioactivity [5]. Material's bioactivity is defined as the ability of apatite to form on their surfaces after immersion in a simulated body fluid (SBF) solution [8]. This effect makes zinc attractive for use as therapeutic agent in the fields of hard tissue regeneration, as dentin [9]. Root dentin undergoes gradual spatial transition in its material properties, and does have regional variations. In the root, a decreasing trend in mineral content from the cervical dentin to the apical dentin has been found [1]. The cervical root dentin is a potential failure site due to deformation, strain and stress concentration [10]. On the other hand, the maximal tensile strength tend to develop in the apical region of the root [7], and instrumenting the apical third reduced the fracture strength of the root [11]. The inner canal wall concentrates the stress distribution to occur in the canal root [7].

Dentin is a mineralized connective tissue that constitutes the bulk of the tooth. Its structure is composed of 70 % inorganic hydroxyapatite (HAp) crystal by weight or 50% HAp crystal by volume, in the form of a sub-micrometer to nanometer-sized carbonate rich, calcium deficient apatite crystallites (~5 x 30 x 100 nm) [12]. The mineral content in dentin consists of crystallites whose size and texture depend on their location in the tooth and maturity of the tissue [13]. The dimensions and morphology of the formed HAp crystallites affect its mechanical properties [14] and may predetermine its clinical service. Shorter and wider crystallites are associated to an increased mineralization, crystallinity and maturity of the formed HAp [15]. The mechanical properties of macroscopic dentin are also strongly dependent on the alignment and orientation of the HAp

crystals [16]. The strain distribution is an important indicator of the stiffness of teeth as force bearing tissue during biting [17]. X-ray diffraction (XRD) represents one of the most powerful techniques to study the hierarchical structure of biological mineral. XRD analysis can be used to perform quantitative measurements of both the crystal orientation and the lattice strain on the tooth surface [17]. In this line, it is recommended to determine the grain size accordingly determined by measuring the deviation of line profile from perfect crystal diffraction, and so the preferred orientation of crystallites. Transmission electron microscopy (TEM) and selected area diffraction patterns (SAED) may be employed to characterize the size, shape and dentin nanostructures.

Thus, the purpose of the present study was to elucidate if the crystallinity and amorphization of radicular dentin is influenced by the treatment with three root canal sealer materials. The null hypothesis is that there are no differences in crystal morphology, structure and texture of radicular dentin treated with three root canal sealing materials.

2. Materials and Methods

2.1. Specimen preparation and cement application

Forty human mandibular premolars with single roots and vital pulp, extracted for orthodontic or periodontal treatments, without caries lesions were obtained with informed consent from donors (18-25 yr of age), under a protocol approved by the Institution Review Board (#139/CEIH/2016). The teeth were randomly selected and stored at 4ºC in 0.5% chloramine T bacteriostatic/bactericidal solution for up to 1 month. This storage medium was replaced weekly. All teeth were integral and examined using a stereomicroscope (Olympus SZ-CTV, Olympus, Tokyo, Japan) to ascertain the absence of any root fracture or craze lines. The teeth were decoronated using a low- speed diamond saw (Accutom-50 Struers, Copenhagen, Denmark), and the root length was standardized to approximately 12 mm. and radiographed at 2 angulations to confirm the presence of a single canal. The root canal treatment began by using Gates Glidden drills (Dentsply Maillefer, Ballaigues, Switzerland), size 2 and 3, in order to shape the coronal third part of the roots. Subsequently, canal patency was achieved using a size 15 Flex-o-file (Dentsply Maillefer, Ballaigues, Switzerland). The working length was measured and established 0.5 mm shorter than apical foramen. The final instrumentation was performed with ProTaper nickel-titanium rotary instruments (Dentsply Maillefer, Ballaigues, Switzerland) up to size F4. At each instrument change, the root canal was irrigated by means of a 27-gauge needle with 0.5 mL of 5% sodium hypochlorite (NaOCl, Panreac, ref. n. 212297), while at the end of canal instrumentation 0.5 mL of a 17% EDTA

solution were used for 1 min (MD-Cleanser, Meta Biomed, Chungbuk, Republic of Korea) to remove the smear layer [18]. Each specimen was finally irrigated with 0.5 mL of 5% NaOCl for 1 min, followed with distilled water for one more minute, and dried with paper points (Dentsply Maillefer). The same operator conducted all procedures.

The specimens were divided randomly into 4 groups (n = 10). Two experimental hydroxyapatite-based cements were used: i) Calcypatite composed by modified hydroxyapatite particles and a calcium hydroxide-based paste and ii) Oxipatite which is a combination of the hydroxyapatite particles and zinc oxide. AH PLUS cement (Dentsply, DeTrey, Konstanz, Germany) was used to form the third group (iii). A control group (iv) in which no sealer was applied was also included, in this control group gutta-percha (GuttaCore) (Dentsply Maillefer, Ballaigues, Switzerland) was compacted into the radicular canal without any sealer or cement. A detailed description of the chemicals and cements is provided in Table 1. Sealers were introduced into the root using a lentulo spiral [19,20], and were compacted into the radicular canal with an endodontic plugger. One size 30 GuttaCore (GC) cone was placed into the canal to working length, in all groups.

The root surface was entirely covered with nail varnish so that only the apical foramen remained exposed [21]. Each tooth was evaluated radiographically at two angulations to confirm the correct placement of the material along the root canal and the absence of voids. Those teeth that did not meet these requirements were replaced by other root canals properly prepared. Finally, the teeth of each cement subgroup were randomly divided in two groups (n=5) and stored in simulated body fluid solution (SBFS) (Table 1) at 37 °C up to fulfill a period of 24 h or 12 m.

After storing, subvolumes were selected to isolate regions in both the cervical section root dentin and apical section root dentin (12 and 4.5 mm respectively, above apex), by sectioning perpendicularly to their long axis into 1 mm ($\pm$0.1 mm) thick slices (Fig. S1). Two dentin disks were obtained from each specimen.

2.2. X-Ray Diffraction (XRD) analysis

Dentin disks were polished using 600, 1200, 2400 and 4000 grit SiC abrasive papers on a water-cooled polishing device (Buehler-MetaDi, Buehler Ltd. Lake Bluff, IL, USA). A final ultrasonic cleaning (10 min) concluded the specimen preparation. Treated surfaces were then submitted to XRD analysis. The X-Ray microdiffractometer (μXRD^2) used in this study was a single crystal diffractometer Bruker D8 Venture (Bruker AXS, Germany) equipped with a 2-dimensional area detector CMOS Photon 100 (Bruker AXS, Germany) and a kappa geometry based goniometer 2D Detector. The X-Ray beam (Cu Kα line, λ=1.5418 Å) was generated

by a Cu microforms source IμS and generator settings of 50 kV/1 mA were employed. The 2D position sensitive detector had 1024x1024 pixels. The beam collimator length was 90 mm and its diameter 0.1 mm (spot size 100 μm). The crystal to detector distance was calibrated with a sample of ylid. The sample was mounted on the XYZ goniometer with the surface to be analyzed placed normal to the φ axis. Then the goniometer is automatically adjusted to bring the sample surface into focus, with the region of interest in the center of the crosshair of the video window by means of a video camera system (NTSC-Digital Video Camera. Model LCL-211H, Watec America Corp.,USA). The considered kappa goniometer positions at 40 mm distance were: 2θ, 40º; ω, 20º; φ, 270º; χ, 50º. All measurements were performed at room temperature (295±0.1°K) and an exposure time of 60.00 s. Three images were obtained from each of the five specimens produced for each experimental group, a total of 15 frames were recorded. The final refined μXRD^2 profile and Debye-Scherrer rings image (pole image) of each group were obtained by accumulating all X-ray energies (wavelengths) in a single image. The results are commonly presented as maximum positions in 2θ (x) and X-ray counts (intensity) (y) in the form of an x-y chart. The XRD2DScan software [22] was employed, as it allows all images to be integrated into a representative single image. The whole batch of the measured frames is loaded and all frames are processed; then a single file is created. This file contains the variation of intensity along the Debye ring associated with the selected reflection as a function of angle, for every processed frame. All this information is used to construct the final refined μXRD^2 profile and pole image.

From the X-ray micro-diffraction pattern, the size and the preferred orientation of the crystallites were calculated [15,23,24]: $d = \frac{K\lambda}{\beta\, cos\theta}$ (1). In this equation d is the mean size of the crystallites, K is a dimensionless shape factor, with a value close to unite –note that in the case of dentin, $K \approx 0.94$ [15], and β is the peak full width at half maximum (FWHM) of the line broadening. In order to obtain the crystallite length and width, this formula was used for the line broadenings corresponding to 002 (H) and 310 (L) reflections, respectively (see data in Table 1). In order to determine the interaction of variables with the HAp structure the ratio H/L [24] was also measured. The preferred orientation of the crystallites (texture) from the following intensity ratios [15]: $R_{hkl} = k_{hkl}\frac{I_{211}}{I_{hkl}}$ (2). In this expression I_{211} and I_{hkl} are the intensities corresponding respectively to line reflections 211 and hkl, and $k_{hkl} = \frac{I^{st}_{hkl}}{I^{st}_{211}}$, where the superscript st refers to intensities calculated according to the JCPDS card [15,25].

2.3. Transmission Electron Microscopy (TEM) analysis

Dentin disks (1mm thickness) were transversally sectioned at three points: 1) in the middle, 2) at both sides right and left about 500 microns from the interface. Specimens were then ground from the external surface (cementum) until a 100 μm distance from the sealer-dentin interface. Grinding was performed by using 600, 1200 and 2400 grit SiC abrasive papers on a water-cooled polishing device (Buehler-MetaDi, Buehler Ltd. Lake Bluff, IL, USA). A final ultrasonic cleaning (10 min) concluded the specimen preparation (Fig S1). Samples were crushed into a fine-grained powder in a liquid nitrogen mortar and pestle, and 2% NaOCl was added to remove the surrounding collagen, with daily changes for a week (using a sonicator). After washing with H_2O and ethanol, the nanocrystals were transferred to a 3 mm diameter carbon/Formvar coated cooper TEM grid [24]. Before analysis, all samples were sputter coated with a thin layer of amorphous carbon. Electron lucent particles were selected by size and distant from grid bars. Stack images were acquired, and the position of the stage was changed between -40 and +50° of α tilt, and collected every 10º. The samples were analyzed using a Transmission Electron Microscope Zeiss Libra 120 (Oberkochen, Germany) at 120 kV in bright-field (BF), and selected area electron diffraction (SAED) patterns were also captured. Normal BF images were produced by tilting the beam to the diffracting plane of interest. Tomographic reconstructions and related data were proceeded with the software iTEM (Olympus Soft Imaging Solutions GmbH, Münster, Germany), comprising acquisition, alignment and visualization. A specific semi-automated modulus for image processing, attached to the microscope, including a 2048x2048 pixel chip BM-2k-120 Dual-Speed on axis SSCCD-camera (TRS, Moorenweis, Germany), was used. Rough images alignment was undertaken on a neighboring crystal, in order to minimize radiation damage. The obtained images were aligned and back projected using the software for 3D from the iTEM tomography extension. Reconstructions were obtained with a silicon graphics workstation self-incorporated.

3. Results

3.1. Micro-X-ray diffraction pattern

The analysis of μXRD^2 profiles of root dentin revealed that the physical broadening (FWHM) of peaks at 002 (2θ, 25.900º; centroid peak position θ_{hkl}, 0/0/-2; I, 10977386) reflection, after observing data plotted by the reduced full width and extended height at half maximum of the phosphate band, was higher (more amorphous) (~1.06 fold) in cervical dentin surfaces treated with both calcypatite and oxipatite when compared with dentin surfaces treated with both GuttaCore and AH Plus, after 12 m of SBFS storage. Differences, practically, did not

appear among groups when apical dentin was assessed, after 12 m time point. Similarly, after 12 m, peaks at 310 (2θ, 40.127º; centroid peak position θ_{hkl}, -3/1/0; I, 1380390) in both cervical and apical dentin surfaces treated with oxipatite showed the lowest FWHM values among groups, denoting a preferred crystalline status. At 002 reflexions analyzed at cervical dentin FWHM increased in oxipatite and calcypatite over time.

At the inner zone of the cervical dentin section, at 002 peak, crystallinity (low FWHM) obtained with the different sealers followed the trend: oxipatite (0.0066) ~ calcypatite (0.0067) < AH Plus (0.0062) = GuttaCore (0.0062) (Fig. 1). The analysis of μXRD^2 profiles displayed high intensity of HAp in samples treated with both calcypatite and oxipatite in cervical dentin at 102, 210, 300, 201, 310 and 321 peaks (Fig. 1). In apical dentin, high intensity of HAp when using both calcypatite and oxipatite was observed at at 211, 112, 300, 201, 310, 222 and 213 peaks (Fig. 2). At the inner zone of the apical dentin, at 310 plane, crystallinity in samples treated with the different sealers followed the trend: oxipatite (0.0210) > calcypatite (0.0220) > AH Plus (0.0236) > GuttaCore (0.0239) (Fig. 2).

3.2. Crystalline size assessment

A qualitative estimation of the size of the coherently scattering domain (*i.e.* the crystallite size) is reported in Table 2. At cervical root dentin, the lowest [τ_{002} (H)] (22.33 nm) crystallite size corresponded to samples treated with calcypatite after 12 m of storage. The longest crystallite size were obtained after using oxipatite at the apical section of root dentin [τ_{002} (H)] (24.15 nm). At cervical root dentin, the narrowest [τ_{310} (L)] (6.46 nm) crystallite size corresponded to dentin treated with AH Plus after 12 m of storage. The widest crystallite size, at the apical section, was obtained after treating dentin surfaces with oxipatite [τ_{310} (L)] (7.36 nm). The ultra-structural observations at 002 reflections of cervical root dentin confirmed that the grain size, expressed throughout the Scherrer-Wilson equation (Eq. 2) of dentin crystals became smaller in samples treated with calcypatite at 12 m storage (21.77 nm). The highest value of grain size appeared after treating the apical dentin with oxipatite (23.53 nm). On the other hand, in both groups of cervical and apical dentin treated with oxipatite, the dentin crystals attained the highest grain size values (6.56 and 6.93 nm, respectively) (Table 2).

3.3. Microstrain assessment

The lattice strain within the long dimension (002 reflection) was lower in case of treating apical dentin with oxipatite ($9.2x10^{-7}$), at 12 m. Cervical and apical dentin halves treated with oxipatite also showed the lowest microstrain values among groups ($1.15x^{10-5}$ and $1.03x^{10-5}$, respectively) within the shortest dimension (310 reflection), at 12 m (Table 2).

3.4. Texture assessment

At 002 plane after 12 m, the texture assessed at the cervical dentin treated with all sealers followed the trend: calcypatite (0.526) > oxipatite (0.480) > GuttaCore (0.400) = AH Plus (0.400). At the apical section of dentin, the trend was: oxipatite (0.590) > AH Plus (0.475) > calcypatite (0.460) > GuttaCore (0.400). At 310 plane after 12 m, the cervical dentin performed as follows: AH Plus (3.74) > GuttaCore (3.61) > calcypatite (3.34) > oxipatite (3.26). At the apical dentin the trend was as follows: GuttaCore (3.74) > AH Plus (3.56) > calcypatite (3.40) > oxipatite (3.28) (Table 2).

3.5. Transmission electron microscopy (TEM) analysis

After 12 m, the cervical dentin section that was treated with calcypatite exhibited, in bright-field (BF), a block-like crystallite morphology (Fig. 3a), while oxipatite-treated dentin showed, at the same location, typical polymorph/polyhedral apatite crystals (Fig. 4a). Calcypatite, at the apical dentin surfaces promoted the formation of plate-like polygons crystallites. They became ordered in agglomerated crystals (Fig. 3c, inset). Views at different tilt angles are shown after tomographic reconstructions at 0º (b), -20º (c), -50º (d), and +20º (e), (Figs. 3). They also were transparent and stable for tilt projections. Oxipatite, at the apical dentin surfaces promoted the formation of multi-domain polycrystalline lattices of overlapped minerals (Fig. 4c, inset). It is shown views at different tilt angles after tomographic reconstructions at 0º (b), -20º (c), -50º (d), and +20º (e) (Figs. 4). They were transparent enough to observe their lattice, and also stable enough for tilt series acquisition (Figs. 4b, 4c, 4d, 4e). Apical dentin treated with AH Plus, at 12 m storage time, showed minerals with typical block-like poly-crystallite morphology (Fig. S2). At cervical dentin, the block-like apatites (Fig. 3a, inset) were confirmed to be more amorphous in nature, with diffuse halos, than that polyhedral apatite morphologies (Fig. 4a, inset). At the apical dentin, polycrystalline lattices reflected a more amorphous matter (Fig. 4f) than that with plate-like polygon morphologies which appeared more crystalline with clear and remarkable halos in the SAED analysis (Figs. 3f, 3g).

4. Discussion

Both HAp-based sealers for endodontic purposes, calcypatite and oxipatite, produced immature crystallites at root cervical dentin, promoting further bioactivity and further dentin remineralization. Oxipatite at root apical dentin provided amorphous and crystalline crystallites, likely associated to high bioactivity and improved mechanical properties. The peak broadening [26] parallel to the *c*-axes [27] [002 plane] in the μXRD^2 that was obtained at cervical dentin when calcypatite and oxipatite were used, at 12 m storage, indicated that a more

amorphous dentin [28] with more crystals imperfections in nanocrystallite materials, *i.e,* small crystallite size and lattice distortion [26] with increased microstrain values (Table 2) is produced.

Reflections at the 002 peak and the corresponding diffraction ring plane (Fig. 1, inset e) clearly establish the lower crystallinity [002 plane] after applying both calcypatite and oxipatite at the inner zone of cervical dentin. The resulted broadening suggests the state of HAp as ultrafine nano-crystalline [29] as it was confirmed in the present study (Table 2), where the Scherrer equation and the Scherrer-Wilson equation [002] attained lower values in samples treated with both HAp-based sealers than with GuttaCore or AH Plus. The association between broadening and poor crystallinity denotes the presence of higher degrees of impurities, amorphous phase and non-stoichiometry [24]. This was linked to a decreased chemical stability and a resulting ion-rich environment with lower mechanical properties [28], likely associated with an increase solubility and improved bioactivity [25]. This amorphization was confirmed after TEM analysis of HAp, in bright-field (BF), which exhibited rounded apatite crystals when calcypatite was applied at cervical dentin (Fig. 3a). These crystals were seem to be more amorphous in nature than the polyhedral apatite which appeared after treating with oxipatite (Fig. 4a) and observing the remarkable halo rings (Fig. 4a, inset) which characterized the crystalline matter.

A qualitative estimation of the size of the coherently scattering domain (*i.e.* the crystallite size) is reported in Table 2, where an increase of the mean crystallite size (~1.04 fold) along a direction perpendicular to the *c*-axis [τ_{310} (*L*)] was obtained when cervical dentin surfaces were treated with oxipatite. Crystallite size in calcified tissues has been shown to increase with tissue maturation [13], which is linked to crystallinity [30]. Nevertheless, τ_{002} (*H*), related to the mean crystallite size along the *c*-axis [24] was slightly lower (~1.02 fold) (Table 2) after treating cervical dentin with calcypatite; as a consequence, shorter and relative wider crystallites resulted after calcypatite-treated cervical dentin (Table 2). Hence, more diffused ring pattern from the SAED analysis was attained in amorphous minerals after treating with calcypatite (Fig. 3a, inset). This amorphization was probably related to the incorporation of carbonate as substituent for PO_4^{-3} in the apatite lattice [31], and became associated to the lowest crystallite size, low *H* and *L* values (22.33nm and 6.69 nm, respectively) in comparison with oxipatite (22.70 nm and 6.97 nm, respectively) at cervical dentin after 12 m storage (Table 2). Therefore, taking into account the present results, it is possible to *i)* associate both lower crystallinity and contraction along the direction orthogonal to the *c*-axis in dentin treated with calcypatite, and *ii)* to partially assume that the higher thickness in crystallites, at dentin treated with oxipatite (6.97 and 7.36 nm at cervical an apical dentin, respectively), fits with a major mineralization and maturity in oxipatite-treated specimens.

Moreover, lower FWHM at τ_{310} (L) (0.0210) was obtained in the oxipatite group if compared to calcypatite-treated specimens (0.0220) (Table 2, Fig.2e).

On the other hand, after 12 m at 310 plane, low FWHM values were obtained when oxipatite and calcypatite were employed (Table 2) at both cervical and apical halves of root dentin, denoting an improved crystallographic or relative atomic order obtained from diffractometry, since narrower peaks suggest less structural variation in both distances and angles [32]. In general, the narrower the spectral peak width is, the higher the degree of mineral crystallinity [33]. The analysis of μXRD^2 profiles confirmed high intensities of samples treated with calcypatite and oxipatite at 211 and 112 peaks at both cervical (Fig. 1) and apical (Fig. 2) root dentin, where diffractography patterns show HAp presence (blue bars) with sharp and narrow crystalline peaks. Similarly, the diffraction analysis formed brighter rings after using calcypatite and oxipatite than in samples treated with GuttaCore and AH Plus (Figs. 1c, 1d, 2c, 2d), indicating lower line broadening of peaks, ~40 counts sharper at apical dentin after (Fig. 2) using HAp-based sealers. Therefore, the null hypothesis must be rejected.

TEM images of HAp, in bright-field (BF), exhibited polyhedral apatite crystals and polycrystalline lattices at cervical (Fig. 4a, inset) and apical (Fig. 4f) dentin halves when oxipatite was used, being not transparent enough to observe their lattice (Fig. 4b), but stable enough for tilt series acquisition (Figs. 4c, 4d, 4e). Three-dimensional reconstructions of one of these particles displayed at different tilt angles permits to carefully examine the different local domains, and their alignment which compose this crystal (Fig. 4c, inset). Nevertheless, at the apical section of dentin treated with oxipatite it is possible to observe, at the same location (Fig. 4a) polycrystalline lattices with mixed (crystalline and amorphous) nature (Fig. 4f).

Texture is the distribution of crystallographic orientation of a polycrystalline sample; it accounts for changes in microstructure, proving a great influence on materials properties, as cracking resistance [34]. Texture indices (R_{hkl}) in dentin polycrystalline structures were calculated according to Eq. (3). For $R\approx1$, the grains were considered randomly oriented [15]. R values greater or lower than 1.0 indicate the presence of preferred grain orientation or texture [25]. At 002 and 310 planes at cervical dentin, samples treated with calcypatite attained the closest values to this number, after 12 m storage, (0.526 and 1.194, respectively); at apical dentin it was oxipatite (0.590 and 1.334, respectively), between HAp-based cement sealers (Table 2). Apical dentin treated with oxipatite attained preferred grain orientation with polycrystalline lattices mixed with amorphous structures at the same location. This is related to both advanced solubility and remineralizing activity [28]. Indices greater than 1 indicate the preferred orientation of the crystallites in the crystallographic direction, at these planes

[15,25]. On the contrary, at the reflections 002 all assessments resulted lower than 1.0 (R<1), but all groups showed less variation than at 310 reflection, *i.e.,* less nano-degradation for the former [25]. In addition, the scarce variation of R values within this reflection mode 002 suggests the existence of a modest gradation in texture at the nanometer scale within the complex dentin microstructure. This means poor three-dimensional interlocking HAp structure to withstand strength and provide both hardness and stress-bearing capability [25]. These are, to the best of our knowledge, the only available results from both μXRD^2 and TEM/SAED combined methodologies relevant to analyze root dentin submitted to different endodontic sealers. Numerically, small changes can be appreciated after analyzing the data. Nevertheless, it should be considered that measurements were performed in biological *ex-vivo* samples and attained differences are consistent with the different applied experimental procedures. Similar magnitude of differences have also been previously reported in previous works [24]. Thereby, this investigation represents the first attempt to assess and interpret the crystal ultrastructure of cervical and apical root dentin. Relative to complementary experimental techniques that ultimately illustrate the clinical outcome of cervical dentin, dark-field TEM (DF-TEM), High Resolution TEM (HRTEM) and Scanning Transmission Electron Microscopy (STEM) should be methodologically incorporated, for future strategies of research.

5. Conclusions

Root cervical dentin treated with hydroxyapatite-based sealers (calcypatite and oxipatite) produced peaks broadening and poor crystallinity of new minerals, which became associated to crystals with high degree of impurities, wide amorphous phase and non-stoichiometry.

At root cervical dentin treated with calcypatite, a promoted preferred grain orientation with shorter and wider crystallite size formation and lower grain size than oxipatite was encountered. It concurred with low tissue maturation and crystallinity in comparison to the dentin treated with Zn-modified hydroxyapatite endodontic cement (oxipatite).

At both root cervical and apical dentin, oxipatite attained improved crystallographic atomic order suggesting less structural variation in both distances and angles. Apical dentin treated with oxipatite attained preferred grain orientation with polycrystalline lattices mixed with amorphous structures at the same location.

Acknowledgements

This work was supported by the Ministry of Economy and Competitiveness (MINECO) and European Regional Development Fund (FEDER) Project MAT2017-85999-P. The authors thank the technical support of Álvaro Carrasco-Carmona for manuscript edition.

References

[1] Kinney JH, Nalla RK, Pople JA, Breunig TM, Ritchie RO. Age-related transparent root dentin: mineral concentration, crystallite size, and mechanical properties. Biomaterials 2005;26:3363–76. https://doi.org/10.1016/j.biomaterials.2004.09.004.

[2] Monticelli F, Sword J, Martin RL, Schuster GS, Weller RN, Ferrari M, et al. Sealing properties of two contemporary single-cone obturation systems. Int Endod J 2007;40:374–85. https://doi.org/10.1111/j.1365-2591.2007.01231.x.

[3] Torabinejad M, Parirokh M, Dummer PMH. Mineral trioxide aggregate and other bioactive endodontic cements: an updated overview – part II: other clinical applications and complications. Int Endod J 2018;51:284–317. https://doi.org/10.1111/iej.12843.

[4] Hakki SS, Bozkurt BS, Ozcopur B, Gandolfi MG, Prati C, Belli S. The response of cementoblasts to calcium phosphate resin-based and calcium silicate-based commercial sealers. Int Endod J 2013;46:242–52. https://doi.org/10.1111/j.1365-2591.2012.02122.x.

[5] Toledano M, Muñoz-Soto E, Aguilera FS, Osorio E, Pérez-Álvarez MC, García-Menocal JAD, et al. The mineralizing effect of zinc oxide-modified hydroxyapatite-based sealer on radicular dentin. Clin Oral Investig 2019; In press. https://doi.org/10.1007/s00784-019-02938-5.

[6] Al-Sanabani JS, Madfa AA, Al-Sanabani FA. Application of calcium phosphate materials in dentistry. Int J Biomater 2013;2013:876132. https://doi.org/10.1155/2013/876132.

[7] Brosh T, Metzger Z, Pilo R. Circumferential root strains generated during lateral compaction with stainless steel vs. nickel-titanium finger spreaders. Eur J Oral Sci 2018;126:518–25. https://doi.org/10.1111/eos.12569.

[8] Kokubo T, Takadama H. How useful is SBF in predicting in vivo bone bioactivity? Biomaterials 2006;27:2907–15. https://doi.org/10.1016/j.biomaterials.2006.01.017.

[9] Matsunaga K. First-principles study of substitutional magnesium and zinc in hydroxyapatite and octacalcium phosphate. J Chem Phys 2008;128:245101. https://doi.org/10.1063/1.2940337.

[10] Kaushik M, Kumar U, Sharma R, Mehra N, Rathi A. Stress distribution in endodontically treated abfracted mandibular premolar restored with different cements and crowns: A three-dimensional finite element analysis. J Conserv Dent 2018;21:557–61. https://doi.org/10.4103/JCD.JCD_206_18.

[11] Patil P, Banga KS, Pawar AM, Pimple S, Ganeshan R. Influence of root canal obturation using gutta-percha with three different sealers on root reinforcement of endodontically treated teeth. An in vitro comparative study of mandibular incisors. J Conserv Dent 2017;20:241–4. https://doi.org/10.4103/JCD.JCD_233_16.

[12] Bertassoni LE, Habelitz S, Pugach M, Soares PC, Marshall SJ, Marshall GW. Evaluation of surface structural and mechanical changes following remineralization of dentin. Scanning 2010;32:312–9. https://doi.org/10.1002/sca.20199.

[13] Toledano M, Aguilera FS, López-López MT, Osorio E, Toledano-Osorio M, Osorio R. Zinc-Containing Restorations Create Amorphous Biogenic Apatite at the Carious Dentin Interface: A X-Ray Diffraction (XRD) Crystal Lattice Analysis. Microsc Microanal 2016;22:1034–46. https://doi.org/10.1017/S1431927616011697.

[14] Feng W, Enyan G, Enmin S, Ping Z, Jinhua L. Structure and properties of bone-like-nanohydroxyapatite/gelatin/polyvinyl alcohol composites. Adv Biosci Biotechnol 2010;1:185–9. https://doi.org/10.4236/abb.2010.13026.

[15] Xue J, Zavgorodniy AV, Kennedy BJ, Swain MV, Li W. X-ray microdiffraction, TEM characterization and texture analysis of human dentin and enamel. J Microsc 2013;251:144–53. https://doi.org/10.1111/jmi.12053.

[16] Sui T, Sandholzer MA, Baimpas N, Dolbnya IP, Walmsley A, Lumley PJ, et al. Multiscale modelling and diffraction-based characterization of elastic behaviour of human dentine. Acta Biomater 2013;9:7937–47. https://doi.org/10.1016/j.actbio.2013.04.020.

[17] Fujisaki K, Todoh M, Niida A, Shibuya R, Kitami S, Tadano S. Orientation and deformation of mineral crystals in tooth surfaces. J Mech Behav Biomed Mater 2012;10:176–82. https://doi.org/10.1016/j.jmbbm.2012.02.025.

[18] Mohammadi Z, Shalavi S, Jafarzadeh H. Ethylenediaminetetraacetic acid in endodontics. Eur J Dent 2013;7:S135–42. https://doi.org/10.4103/1305-7456.119091.

[19] Mestres G, Aguilera FS, Manzanares N, Sauro S, Osorio R, Toledano M, et al. Magnesium phosphate cements for endodontic applications with improved long-term sealing ability. Int Endod J 2014;47:127–39. https://doi.org/10.1111/iej.12123.

[20] Monticelli F, Osorio R, Toledano M, Ferrari M, Pashley DH, Tay FR. Sealing properties of one-step root-filling fibre post-obturators vs. two-step delayed fibre post-placement. J Dent 2010;38:547–52. https://doi.org/10.1016/j.jdent.2010.03.014.

[21] Bouillaguet S, Shaw L, Barthelemy J, Krejci I, Wataha JC. Long-term sealing ability of Pulp Canal Sealer, AH-Plus, GuttaFlow and Epiphany. Int Endod J 2008;41:219–26. https://doi.org/10.1111/j.1365-2591.2007.01343.x.

[22] Rodriguez-Navarro AB. Registering pole figures using an X-ray single-crystal diffractometer equipped with an area detector. J Appl Crystallogr 2007;40:631–4. https://doi.org/10.1107/S0021889807014574.

[23] Perales F, Agulló-Rueda F, Lamela J, Heras C de las. Optical and structural properties of Sb2S3/MgF2 multilayers for laser applications. J Phys Appl Phys 2008;41:045403. https://doi.org/10.1088/0022-3727/41/4/045403.

[24] Toledano M, Aguilera FS, Osorio E, López-López MT, Cabello I, Toledano-Osorio M, et al. Submicron-to-nanoscale structure characterization and organization of crystals in dentin bioapatites. RSC Adv 2016;6:45265–78. https://doi.org/10.1039/C6RA02373H.

[25] Low I-M. Depth-Profiling of Crystal Structure, Texture, and Microhardness in a Functionally Graded Tooth Enamel. J Am Ceram Soc 2004;87:2125–31. https://doi.org/10.1111/j.1151-2916.2004.tb06369.x.

[26] Zhang Z, Zhou F, Lavernia EJ. On the analysis of grain size in bulk nanocrystalline materials via x-ray diffraction. Metall Mater Trans A 2003;34:1349–55. https://doi.org/10.1007/s11661-003-0246-2.

[27] Mürer FK, Sanchez S, Álvarez-Murga M, Michiel MD, Pfeiffer F, Bech M, et al. 3D Maps of Mineral Composition and Hydroxyapatite Orientation in Fossil Bone Samples Obtained by X-ray Diffraction Computed Tomography. Sci Rep 2018;8:10052. https://doi.org/10.1038/s41598-018-28269-1.

[28] Moshaverinia A, Ansari S, Moshaverinia M, Roohpour N, Darr JA, Rehman I. Effects of incorporation of hydroxyapatite and fluoroapatite nanobioceramics into conventional glass ionomer cements (GIC). Acta Biomater 2008;4:432–40. https://doi.org/10.1016/j.actbio.2007.07.011.

[29] Liu Y, Huang J, Li H. Synthesis of hydroxyapatite-reduced graphite oxide nanocomposites for biomedical applications: oriented nucleation and epitaxial growth of hydroxyapatite. J Mater Chem B 2013;1:1826–34. https://doi.org/10.1039/C3TB00531C.

[30] Olszta MJ, Cheng X, Jee SS, Kumar R, Kim Y-Y, Kaufman MJ, et al. Bone structure and formation: A new perspective. Mater Sci Eng R Rep 2007;58:77–116. https://doi.org/10.1016/j.mser.2007.05.001.

[31] Toledano M, Osorio E, Aguilera FS, Cabello I, Toledano-Osorio M, Osorio R. Ex vivo detection and characterization of remineralized carious dentin, by nanoindentation and single point Raman spectroscopy, after amalgam restoration. J Raman Spectrosc 2017;48:384–92. https://doi.org/10.1002/jrs.5055.

[32] Schwartz AG, Pasteris JD, Genin GM, Daulton TL, Stavros Thomopoulos. Mineral distributions at the developing tendon enthesis. PloS One 2012;7:e48630. https://doi.org/10.1371/journal.pone.0048630.

[33] Karan K, Yao X, Xu C, Wang Y. Chemical profile of the dentin substrate in non-carious cervical lesions. Dent Mater 2009;25:1205–12. https://doi.org/10.1016/j.dental.2009.04.006.

[34] Liss K-D, Bartels A, Schreyer A, Clemens H. High-energy X-rays: a tool for advanced bulk investigations in materials science and physics. Textures Microstruct 2003;35:219–52. https://doi.org/10.1080/07303300310001634952.

Figure and table captions

Fig. 1. Refined μXRD^2 profiles of the inner zone at the cervical dentin after 12 m of SBFS storage. The Debye-Scherrer rings are shown in inset (a) GuttaCore, (b) AH Plus, (c) calcypatite and (d) oxipatite. Pointers and double arrows mean weak and strong diffraction rings, respectively. Vertical bars represent HAp peaks. Inset (e) represents a truncated μXRD^2 profile after observing the reflection at 002 peak and further full width half maximum (FWHM) measurements.

Fig. 2. Refined μXRD^2 profiles of the inner zone of the apical dentin after 12 m of SBFS storage. The Debye-Scherrer rings are shown in inset (a) GuttaCore, (b) AH Plus, (c) calcypatite and (d) oxipatite. Pointers and double arrows mean weak and strong diffraction rings, respectively. Vertical bars represent HAp peaks. Inset (e) represents a truncated μXRD^2 profile after observing the reflection at 310 peak and further full width half maximum (FWHM) measurements.

Fig. 3. (a) Bright-field of an assembly of a block-like or rounded apatite crystals of cervical root dentin, at the inner zone treated with calcypatite, after 12 m storage. It is observed that the particles have a domain of locally aligned crystal arrays, showing the staggered order of polygon crystallites (scale bar: 0.2 μm). The inset (top left), corresponds to a selected area electron diffraction (SAED) d-values of submicron size (+). Diffractography depicts diffuse halo rings, indicating the presence of amorphous structure. (b to e) Bright-field of an assembly of polymorphic apatite crystals of overlapped minerals of apical root dentin, at the inner zone treated with calcypatite, after 12 m storage. Agglomerated crystals of plate-like polygon crystallites characterized these hexagonal minerals (scale bar: 0.5 μm). The collage shows views at different tilt angles after tomographic reconstructions at (b) 0º, (c) -20º, (d) -50º, and (e) +20º. [(f) ✚ in b, (g) ✖ in b], (b), Selected area electron diffractions (SAED) of the crystals shown at microscale. They exhibit clear halo rings and diffraction *d* spacing values of submicron size crystals (nm^{-1}), indicating the presence of crystalline matter, whose pattern show relatively uniform reflections for all variants. They also confirm the presence of hexagonal apatite and a highly polycrystalline structure. (f) and (g), Regions for SAED analysis (h·I, h·II), respectively.

Fig. 4. (a), Bright-field of an assembly of polyhedral apatite crystals of cervical root dentin, at the inner zone treated with oxipatite, after 12 m storage. The minerals have multiple domains of locally aligned crystal arrays with tendency to agglomerate. Profiles at A were highlighted to remark the overlapping (scale bar: 0.5 μm). The inset (top left), shows a selected area electron diffraction (SAED) pattern containing differentiated halo rings and clear *d* spacing values, meaning the presence of remnant crystallite matter. (b to e) Bright-field of an

assembly of polycrystalline lattices of overlapped minerals of apical root dentin, at the inner zone treated with oxipatite, after 12 m storage. The mineral showed the in detailed polyhedral apatite appearance of crystallites (scale bar: 0.2 μm).The collage shows views at different tilt angles after tomographic reconstructions at (b) 0º, (c) -20º, (d) -50º, and (e) +20º. (f), Diffraction pattern with clear central halo rings and *d* spacing values, meaning the presence of remnant crystallite structure. Peripheral diffuse halo rings can be noted at the external orbits of the selected area electron diffraction pattern (SAED) indicating amorphous structure. This figure represents zone axis patterns in which the matrix reflections are intense. The presence of crystals less than micron size (nm^{-1}) is provided.

Table 1. Materials and chemicals used in this study.

Table 2. Micro-X-ray diffraction pattern analysis at the different experimental groups.

Figure 1

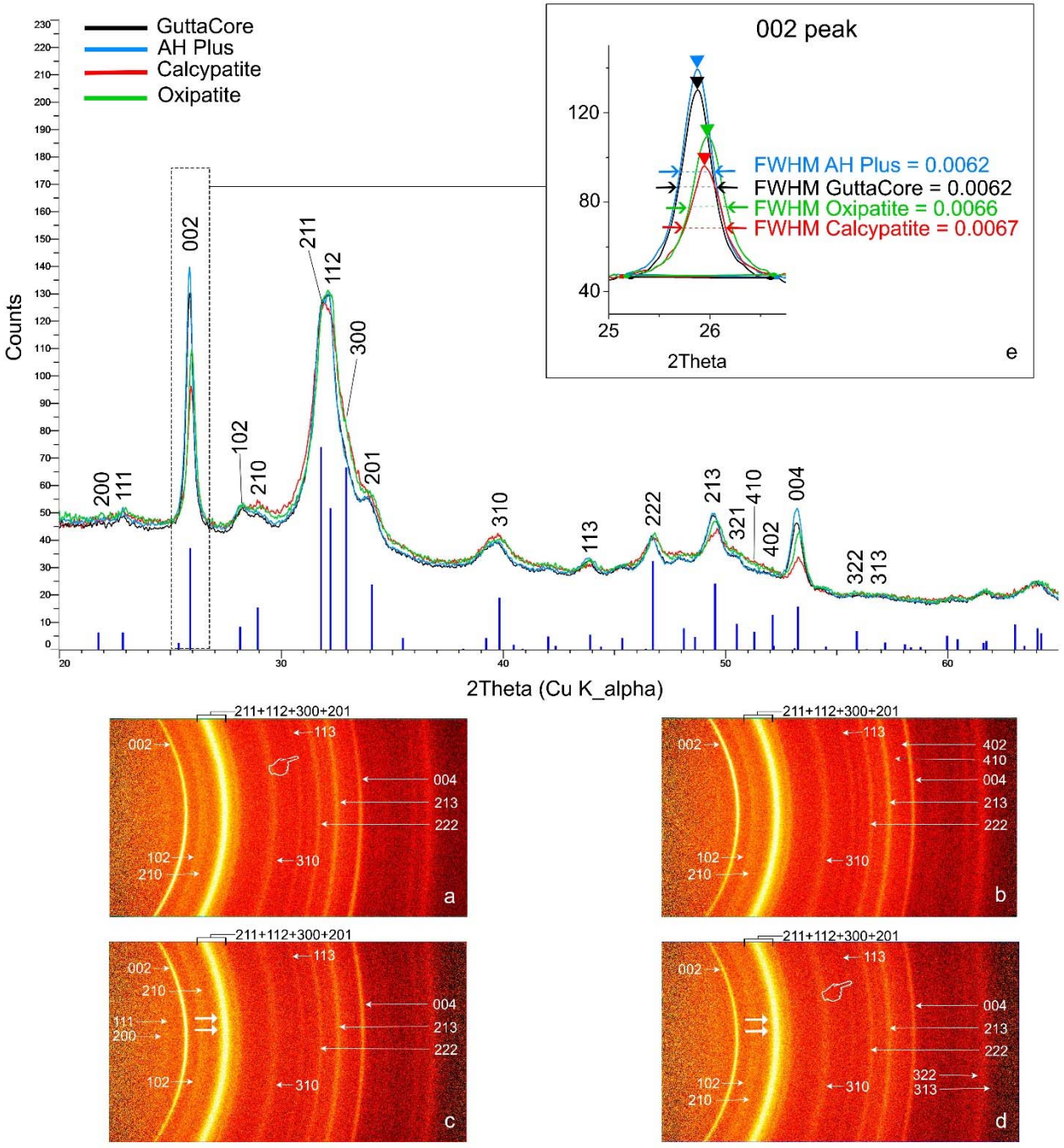
GuttaCore
AH Plus
Calcypatite
Oxipatite
Counts
2Theta (Cu K_alpha)
002
200
111
102
210
211
112
300
201
310
113
222
213
321
410
402
004
322
313
002 peak
FWHM AH Plus = 0.0062
FWHM GuttaCore = 0.0062
FWHM Oxipatite = 0.0066
FWHM Calcypatite = 0.0067
2Theta
e
211+112+300+201
a
b
c
d

Figure 2

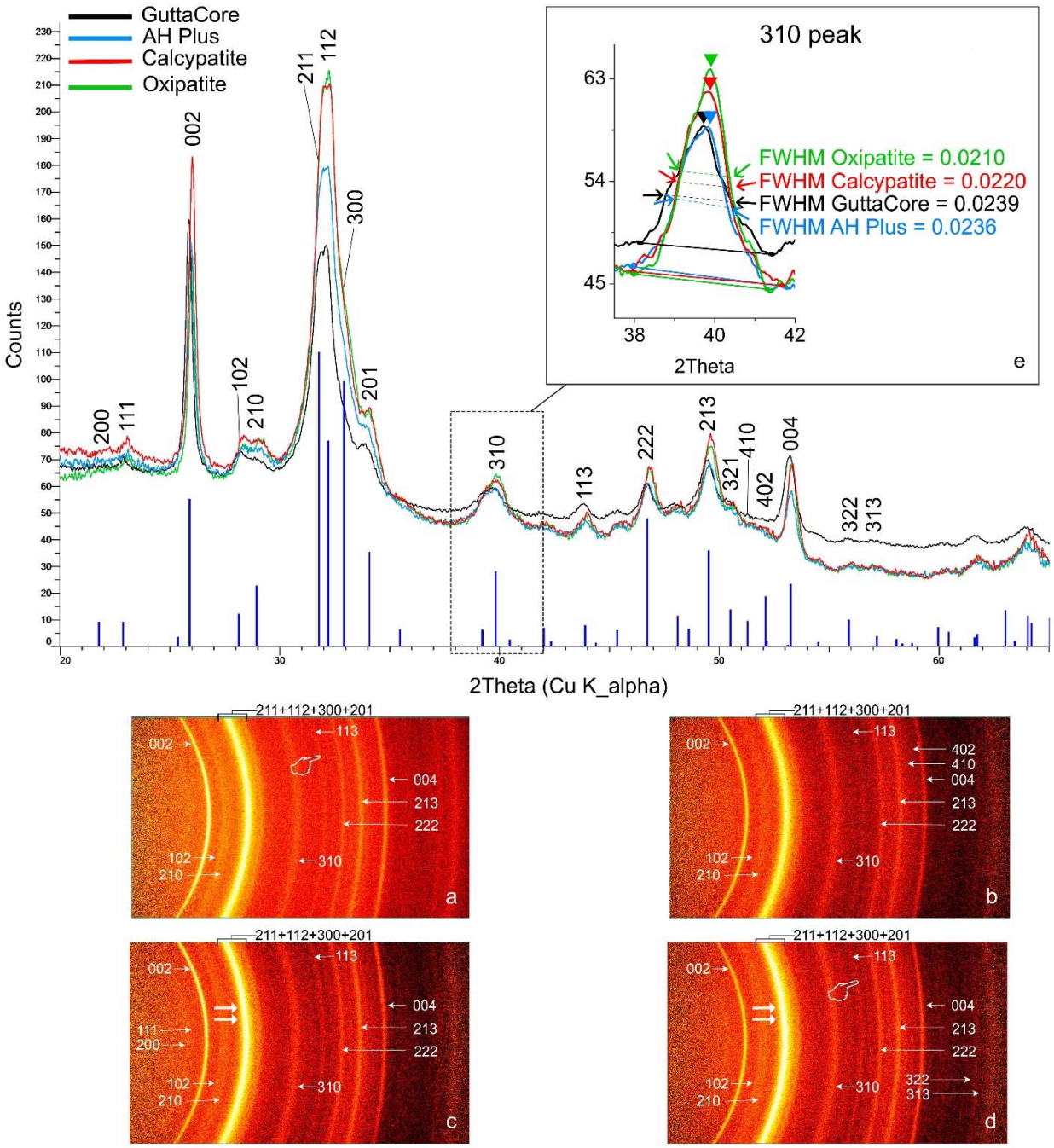
GuttaCore
AH Plus
Calcypatite
Oxipatite
Counts
2Theta (Cu K_alpha)
200
111
002
102
210
211
112
300
201
310
113
222
213
321
410
004
322
313
310 peak
FWHM Oxipatite = 0.0210
FWHM Calcypatite = 0.0220
FWHM GuttaCore = 0.0239
FWHM AH Plus = 0.0236
2Theta
e
211+112+300+201
a
b
c
d

Figure 3

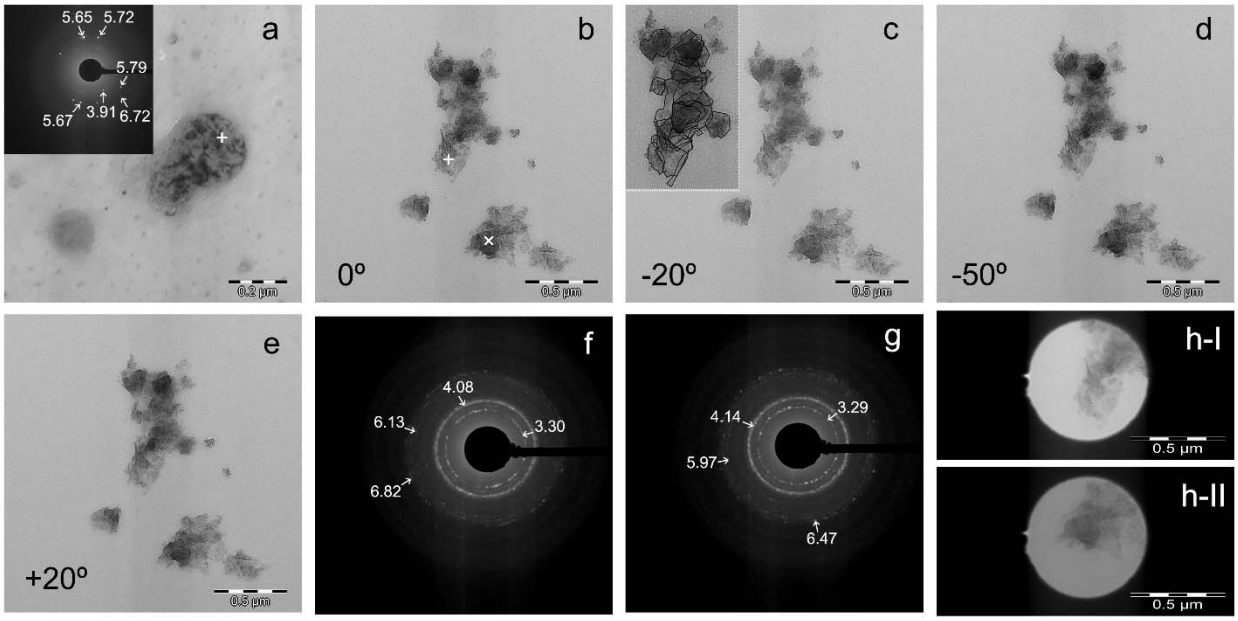

Figure 4

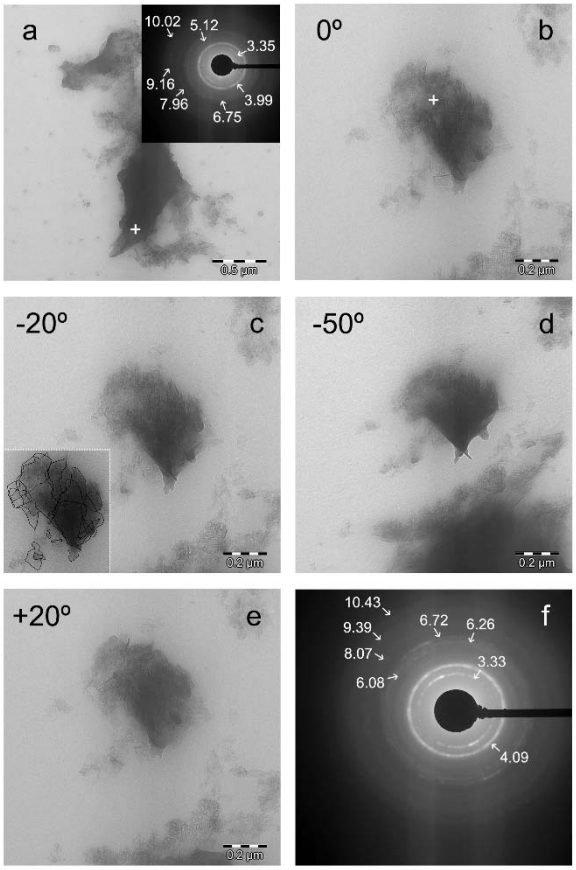

Table 1.

Product details			
Calcypatite	Calcium hydroxide $(CaOH)_2$	**Basic formulation per 100 gr**	
		Content and quantity (g)	*Percentage (%)*
		Calcium hydroxide 45.0 g Carbowax 400 40.0 g Titanium dioxide 7.0 g Aerosil 1.0 g Barium Sulphate 7.0 g	42.5
	Hydroxyapatite modified particles	*Component and percentage* Calcium 39.2 % Phosphorus 18.3 % Magnesium < 0.1 % Sodium < 0.1 % Silicon 0.001-0.03 % Other minor components < 0.005 % *Molar relation Ca/P 1.66*	57.5
Oxiapatite	Zinc oxide (ZnO)	**Basic formulation per 100 gr**	
		Content and quantity (g)	*Percentage (%)*
		Zinc oxide (ZnO) 39.61 g Titanium dioxide 5.8 g Carbowax 400 40.0 g Aerosil 2.0 g Barium sulphate 14.8 g	42.5
	Hydroxyapatite modified particles	*Component and percentage* Calcium 39.2 % Phosphorus 18.3 % Magnesium < 0.1 % Sodium < 0.1 % Silicon 0.001-0.03 % Other minor components < 0.005 % *Molar relation Ca/P 1.66*	57.5
AH Plus (Dentsply, DeTrey, Konstanz, Germany)		Paste A: diepoxide, calcium tungstate, zirconium oxide, aerosil, pigment (Fe oxide) Paste B: 1-adamantane amine, N,N'-dibenzyl-5-oxa-nonandiamine-1,9, TCD-Diamine, calcium tungstate, zirconium oxide, aerosil, silicone oil	
GuttaCore (Dentsply Tulsa Dental Specialties, Tulsa, USA)		Gutta-percha; zinc oxide; bismuth oxide; 2,5-dimethyl-2,5di(tertbutylperoxy)hexane; titanium dioxide; para-amid fiber; silica,amorphous, precipitated; other components (<5%)	
NaOCl 5% (Panreac Química SA, Barcelona, Spain)			
EDTA 17% (Sigma Aldrich, St. Louis, MO, USA)			
Simulated Body Fluid Solution (SBFS) pH=7.45	Sigma Aldrich, St. Louis, MO, USA	NaCl 8.035 g $NaHCO_3$ 0.355 g $K_2HPO_4 \cdot 3H_2O$ 0.231 g, $MgCl_2 \cdot 6H_2O$ 0.311 g 1.0 M – HCl 39 ml Tris 6.118 g	
	Panreac Química SA, Barcelona, Spain	KCl 0.225 g $CaCl_2$ 0.292 g Na_2SO_4 0.072 g 1.0 M – HCl 0–5 ml	

Abbreviations: SBFS: simulated body fluid solution; TCD: 3(4),8(9)-bis(aminomethyl)triciclo[5.2.1.02,6] Decane; NaCl: sodium chloride; $NaHCO_3$: sodium bicarbonate; KCl: potassium chloride; $K_2HPO_4 \cdot 3H_2O$: potassium

phosphate dibasic trihydrate; $MgCl_2 \cdot 6H_2O$: magnesium chloride hexahydrate; HCl: hydrogen chloride; $CaCl_2$: Calcium chloride; Na_2SO_4: sodium sulfate; Tris: tris(hydroxylmethyl) aminomethane.

Table 2.

			002 plane					310 plane					
	Disk	**Storage time**	**FWHM**	***H*: Scherrer equation (nm) (τ) (crystallite size)**	**Scherrer-Wilson equation (nm)(Grain size)**	**Microstrain %**	**R_{hkl}**	**FWHM**	***L*: Scherrer equation (nm) (τ) (crystallite size)**	**Scherrer-Wilson equation (nm) (Grain size)**	**Microstrain %**	**R_{hkl}**	***H/L***
GuttaCore	Cervical	24h	0.0061	24.58	23.96	$8.9x10^{-7}$	0.435	0.0244	6.31	5.95	$1.40x10^{-5}$	1.323	3.89
		12m	0.0062	23.83	23.23	$9.5x10^{-7}$	0.400	0.0233	6.60	6.22	$1.28x10^{-5}$	1.326	3.61
	Apical	24h	0.0060	24.89	24.26	$8.7x10^{-7}$	0.451	0.0228	6.75	6.36	$1.23x10^{-5}$	1.189	3.69
		12m	0.0062	24.12	23.52	$9.3x10^{-7}$	0.400	0.0239	6.46	6.08	$1.34x10^{-5}$	1.415	3.74
AH Plus	Cervical	24h	0.0070	21.30	20.77	$1.2x10^{-6}$	0.465	0.0227	6.79	6.40	$1.34x10^{-5}$	1.388	3.14
		12m	0.0062	24.12	23.52	$9.3x10^{-7}$	0.400	0.0239	6.46	6.08	$1.34x10^{-5}$	1.415	3.74
	Apical	24h	0.0063	23.78	23.18	$9.5x10^{-7}$	0.400	0.0219	7.04	6.63	$1.13x10^{-5}$	1.369	3.38
		12m	0.0064	23.28	22.70	$9.9x10^{-7}$	0.475	0.0236	6.54	6.16	$1.31x10^{-5}$	1.210	3.56
Calcypatite	Cervical	24h	0.0061	24.51	23.89	$9.0x10^{-7}$	0.405	0.0215	7.19	6.77	$1.08x10^{-5}$	1.402	3.41
		12m	0.0067	22.33	21.77	$10.8x10^{-7}$	0.526	0.023	6.69	6.30	$1.25x10^{-5}$	1.194	3.34
	Apical	24h	0.0060	24.77	24.14	$8.8x10^{-7}$	0.400	0.021	7.39	6.96	$1.02x10^{-5}$	1.510	3.35
		12m	0.0063	23.70	23.10	$9.6x10^{-7}$	0.460	0.022	6.97	6.56	$1.15x10^{-5}$	1.350	3.40
Oxipatite	Cervical	24h	0.0064	23.38	22.79	$10.0x10^{-7}$	0.427	0.022	6.97	6.57	$1.15x10^{-5}$	1.265	3.35
		12m	0.0066	22.70	22.13	$10.5x10^{-7}$	0.480	0.022	6.97	6.56	$1.15x10^{-5}$	1.286	3.26
	Apical	24h	0.0063	23.80	23.19	$9.5x10^{-7}$	0.443	0.022	6.95	6.55	$1.15x10^{-5}$	1.332	3.42
		12m	0.0062	24.15	23.53	$9.2x10^{-7}$	0.590	0.021	7.36	6.93	$1.03x10^{-5}$	1.334	3.28

Abbreviations: FWHM, Full-width half-maximum; R_{hkl}, Texture (preferred orientation of the crystallites).

Supporting Information

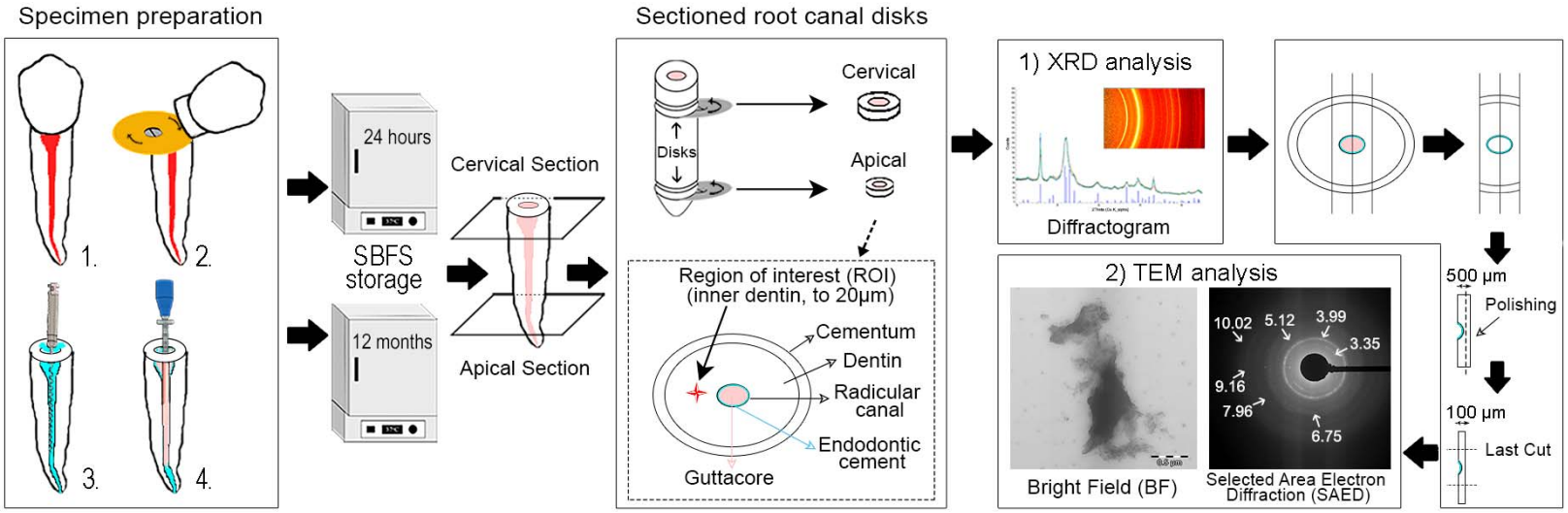

Fig. S1. Scheme of the methodology followed in this study: single root premolars were selected (1), decoronated (2), and endodontically treated. Abbreviations: SBFS: simulated body fluid solution; XRD: X-Ray Diffraction; TEM: Transmission Electron Microscopy. ✦Indicates distance from the radicular canal wall.

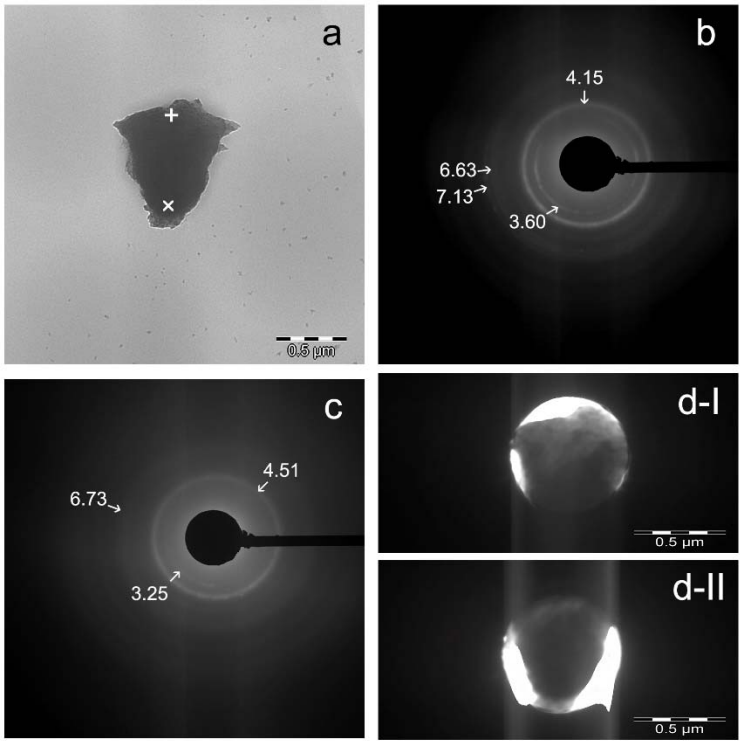

Fig. S2. Bright-field of an assembly of polyhedral apatite crystals of overlapped minerals of apical root dentin, at the inner zone treated with AH Plus, after 12 m storage. (a) Minerals showed a typical block-like poly-crystallite morphology (scale bar: 0.5 µm). (b, c) A selected area electron diffraction (SAED) pattern of the crystals exposed in d·I (✚ in A) and d·II (✖ in A) at nanoscale, respectively. The two relatively diffuse halo rings, indicate the presence of some amorphous remnant structure.